ADVANCED MATERIALS
www.advmat.de

Hierarchical Porous Graphene/Polyaniline Composite Film with Superior Rate Performance for Flexible Supercapacitors

Yuena Meng, Kai Wang, Yajie Zhang, and Zhixiang Wei**

Supercapacitors, as clean energy-storage devices, have attracted great attention owing to their high power density, long cycling life, and high charge–discharge rate.[1] Supercapacitors have been used in many critical areas, such as electrical vehicles, power grids, and aerospace applications.[2] With the growing demand for portable and wearable energy-storage systems, the flexible supercapacitor is gaining more and more interest.[3] Graphene, which consists of a monolayer or a few atomic layers only of graphite, has many special properties, such as high theoretical specific area, high electrical conductivity, and superior mechanical properties, as well as a low fabrication cost. Thus, graphene is regarded as one of the best candidates for flexible electrode materials.[4] Much effort has been focused on designing graphene into various flexible structures, such as graphene paper, [4b,c,5] graphene gel,[6] transparent electrodes,[7] and so on. However, because of the aggregating nature of graphene due to strong π–π interactions, the large surface area cannot be fully utilized, especially at a high charge–discharge rate. To overcome the overstacking problems of graphene sheets and obtain high rate performance in supercapacitors, various three-dimensional (3D) graphene bulk materials have been developed.[8] Generally, 3D graphene is a structure which contains interconnected pores that prevent the restacking of graphene sheets. For instance, Cheng and co-workers reported graphene networks produced by using a chemical vapor deposition (CVD) and template method[9] and Shi and co-workers prepared a self-assembled graphene hydrogel by a hydrothermal method.[8c] However, reports on 3D graphene porous films with high flexibility, which can be directly used as an electrode without additional transfer substrates, are few. Thus, maintaining the flexibility of graphene and preventing it from self-stacking remain important scientific challenges.

When being used as an electrode material for supercapacitors, the capacitance of graphene is stable but relatively low (around 100 to 200 F g^{-1}) because it mainly stores energy through the electric double-layer capacitor mechanism.[8b,10] Pseudocapacitance materials are alternative electrode materials based on a Faradic mechanism and these have much higher specific capacitance but poor stability.[11] To combine the virtues of the two types of materials, composites of graphene and nanostructured pseudocapacitance materials were prepared and studied.[12] Polyaniline (PANI) is one of the best candidates for supercapacitors among pseudocapacitance materials. PANI has good environmental stability, a unique conducting mechanism, and unusual doping/dedoping chemistry.[13] PANI nanowires provide high pseudocapacitance, higher surface area than the bulk material, and an optimized ion-diffusion pathway, which thus improves their supercapacitor performance over that of the bulk material. The specific capacitance of PANI nanowire arrays has measured as high as 950 F g^{-1} in a three-electrode system.[14] When in a composite with graphene oxide (GO) nanosheets, these electrode materials exhibit a synergistic effect of carbonaceous nanomaterials and conducting polymers.[15]

Herein, we describe the design and preparation of a free-standing porous graphene film (3D-RGO) by a facile template method. 3D-RGO film possesses unique features of both an interconnected porous structure and high flexibility. The formation of interconnected pores facilitates the access of electrolyte ions to the internal surface of the graphene film, which guarantees a high charge–discharge rate performance. Such a structure is also easy to composite with other functional materials. A hierarchical composite film with PANI nanowire arrays (3D-RGO/PANI) was further produced to combine the advantages of both materials. 3D-RGO and 3D-RGO/PANI both showed superior rate performance to that of stacked graphene sheets when used as electrode materials of supercapacitors, and the 3D-RGO/PANI film exhibited higher capacitance than 3D-RGO because of the pseudocapacitance of PANI.

To obtain a 3D-RGO film with high flexibility and interconnected pores, $CaCO_3$ particles formed in situ in GO dispersion were used as a template to facilitate the formation of a porous structure. The thickness of most GO sheets was observed to be ca. 1.0 nm (see Figure S1 in Supporting Information), which corresponds well with the thickness of one individual layer of GO. Although polymer microspheres have also been used as a sacrificial template to produce porous structures, the dissolution of polymer microspheres normally needs a large amount of organic solvent.[16] $CaCO_3$ is a sacrificial template that can be removed easily by dilute acidic solution. **Figure 1** illustrates the preparation of 3D-RGO and 3D-RGO/PANI. First, $CaCl_2$ was added to a GO dispersion to form a uniform mixture (Figure 1a). With CO_2 bubbling through the mixture, $CaCO_3$ particles were formed and wrapped with GO sheets in situ. A composite film of GO and $CaCO_3$ was obtained by vacuum

Y. N. Meng, Dr. K. Wang, Dr. Y. J. Zhang, Prof. Z. X. Wei
National Center for Nanoscience and Technology
No.11 Beiyitiao, Zhongguancun
Beijing, 100190, P. R. China
E-mail: zhangyj@nanoctr.cn; weizx@nanoctr.cn
Y. N. Meng
Academy for Advanced Interdisciplinary Studies
Peking University
No. 5 Yiheyuan Road Haidian District
Beijing, 100871, P. R. China

DOI: 10.1002/adma.201303529

ADVANCED MATERIALS
www.advmat.de

www.MaterialsViews.com

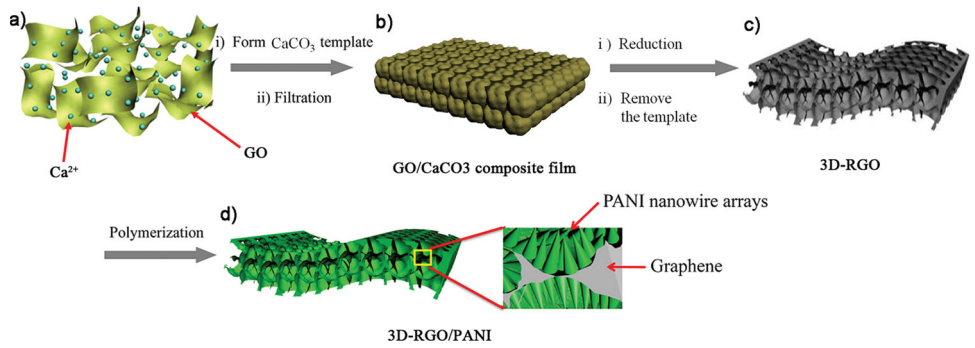

Figure 1. Preparation of the 3D-RGO and 3D-RGO/PANI films. a) Uniform dispersion of GO containing Ca^{2+}. b) GO/$CaCO_3$ composite film formed by $CaCO_3$ precipitation and then filtration c) flexible 3D graphene film with interconnected pores by reduction and $CaCO_3$ removal; d) hierarchical PANI/graphene composites formed by the polymerization of PANI nanowire arrays.

filtration (Figure 1b). When GO was reduced using hydrazine vapor and then $CaCO_3$ was removed by washing with dilute acid, a bendable 3D-RGO skeleton was produced (Figure 1c). By using this skeleton as a substrate, PANI nanowire arrays were grown on the outer and inner surface of 3D-RGO by a dilute polymerization process,[17] thus yielding a hierarchical 3D-RGO/PANI composite film (Figure 1d).

The digital image in **Figure 2**a shows a free-standing film of 3D-RGO with dark-gray color and relatively low reflectivity. As shown in the inserted picture, the film has very good flexibility and can be easily bent. The area density of the film is about 0.25 mg cm^{-2}, which demonstrates the lightness of the film.[18] Scanning electron microscopy (SEM) images of the free-standing RGO film are shown in Figure 2b and 2c. An interconnected 3D network structure can be clearly observed from the cross-section of the film (Figure 2b, and Figure S2). The thickness of the whole film is about 50 μm. The magnified image (Figure 2c) shows the graphene sheets crumpled with some wrinkles on their surfaces, which form pores of several micrometers. The pores are interconnected to one another, which is facilitated with other functional materials. The pore walls are ultrathin, consisting of a few layers of partially stacked graphene sheets, which ensures good mechanical properties for the flexible film.[19] The Brunauer–Emmett–Teller (BET) result shows that the specific surface area of 3D-RGO is 116.2 m^2 g^{-1}. The formation of such a structure is mainly attributed to the presence of $CaCO_3$. $CaCO_3$ particles were synthesized in the presence of GO.[20] After standing overnight, the phase of $CaCO_3$ changed from vaterite to calcite,[21] still with GO sheets tightly interwoven. The irregular shape of the calcite particles facilitated the formation of the free-standing film. Upon the removal of $CaCO_3$, the formed graphene pores preserved the shape of the $CaCO_3$ particles, forming an interconnected macroporous structure. Thus, a 2D-structured graphene sheet formed so-called 3D porous structures,[8d,22] leading to a free-standing porous film.

PANI nanowires were grown by a dilute polymerization procedure.[15a,17] As the PANI nanowire arrays were grown on the graphene sheet of 3D-RGO, the film slightly darkened in color while still preserving good bendability (see Figure S3).

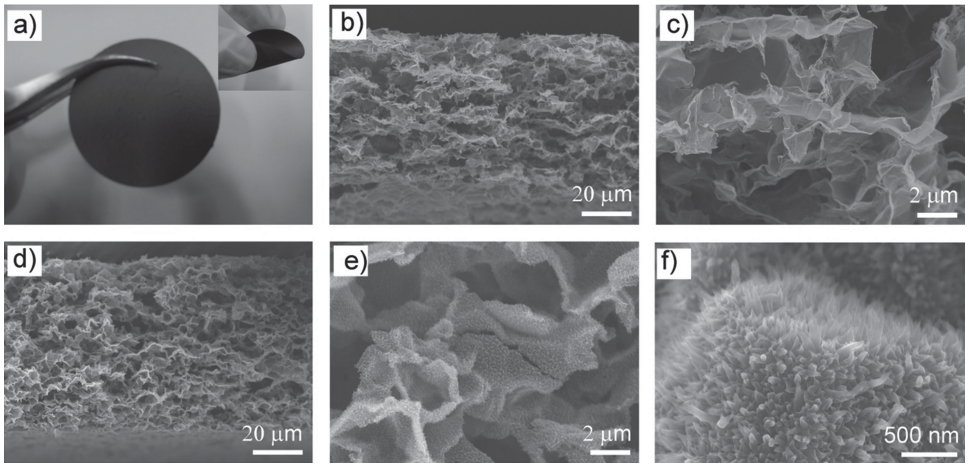

Figure 2. Morphologies and structures of the 3D-RGO and 3D-RGO/PANI films. a) Digital images, with the inserted image showing the flexibility of the film; b,c) SEM images of a cross-section of 3D-RGO film at different magnifications; d–f) cross-section of the hierarchical composite film at different magnifications.

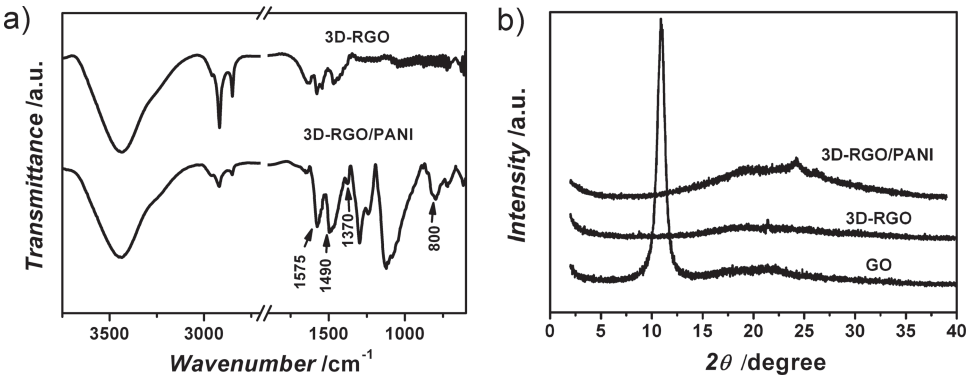

Figure 3. Characterization of the 3D-RGO and 3D-RGO/PANI films. a) FTIR spectra; b) XRD patterns.

The weight ratio of PANI to RGO in the porous hierarchical 3D-RGO/PANI material was calculated as ca. 4.1. The interconnected channels of 3D-RGO were available to aniline diffusion, and a low concentration of aniline in the polymerization process guaranteed a well-controlled nucleation–growth condition for the PANI nanowires. Therefore, vertically aligned nanowire arrays were obtained on the graphene surface of 3D-RGO (Figure 2d to 2f). PANI nanoarrays grow not only on the outer surface but also on the interior surface of graphene in the free-standing film. [17] The film showed a hierarchical structure while maintaining interconnected 3D pores, which facilitated ion diffusion when the film was used as an electrode.

The structures of the 3D-RGO and 3D-RGO/PANI films were investigated using Fourier-transform infrared (FTIR) spectroscopy and X-ray diffraction (XRD; **Figure 3**). The FTIR spectrum of the 3D-RGO film (Figure 3a) displayed obvious peaks at 3436, 2918, and 2850 cm^{-1}, which correspond to –OH, –C–H, and $–(C–H)_n$ stretching vibrations, respectively. These results are attributed to the presence of partially reduced GO (RGO) sheets. The reduction of GO is further confirmed by X-ray photoelectric spectroscopy (XPS). The C1s signals contributed by the C=O and C–O groups were significantly decreased after reduction, which indicates that most of these groups were reduced (see Figure S4). Compared with the FTIR spectrum of the 3D-RGO film, several new peaks attributed to PANI were found in the spectrum of the composite film (Figure 3a). The new peaks at 1575, 1490, 1370, and 800 cm^{-1} were attributed to the vibrations of –C=N, –C=C, –C–N, and –C–H, respectively, which demonstrates the combination of PANI with the reduced graphene sheets.[23]

The combination of RGO and PANI was further confirmed by XRD. Graphite is characterized by a sharp (002) peak at around $2\theta = 26.50°$ with a typical interlayer spacing of 0.335 nm.[24] The interlayer spacing of GO used in this work was calculated to be 0.80 nm, with an intense peak centered at $2\theta = 11°$ (Figure 3b) that fits well with reported results.[25] A broad peak can be observed from 15° to 25° in the XRD pattern of the 3D-RGO film, which indicates the existence of weak π–π stacking between the graphene sheets. This result demonstrates that in the as-prepared 3D-RGO film, RGO sheets are mainly randomly oriented and graphene sheets are poorly ordered along the stacking direction, which results in the formation of a 3D network structure. In the case of the 3D-RGO/PANI composite film, two new broad peaks centered at $2\theta = 20.12°$ and 25.21° can be found in the XRD pattern, which are characteristic of PANI nanowires[26] and, therefore, indicate the formation of PANI in the hierarchical 3D-RGO/PANI composite.

The supercapacitor performances of the as-prepared 3D-RGO and its composite film were evaluated by means of cyclic voltammetry (CV), galvanostatic charge–discharge, electrochemical impedance spectroscopy (EIS), and cycling-life tests in two-electrode systems (**Figure 4**).[27] For comparison, a closely packed RGO film was prepared by vacuum filtering reduction of the same amount of GO dispersion (preparation and SEM images of the RGO film are given in Figure S5). The 3D-RGO and 3D-RGO/PANI free-standing film were cut into round slices of electrode and tested in Swagelok-type cells at room temperature. Without the addition of binding agent or conductive additive, such small pieces of film can maintain good mechanical strength.

The CV curves of the RGO and 3D-RGO films were nearly rectangular in shape (Figure 4a), which characterizes the formation of an electrical double layer to store energy. The area of each closed CV curve suggests its specific capacitance. The specific capacitance of the 3D-RGO, as expected, was much larger than that of RGO film. When the graphene sheets form a 3D porous structure, the effective specific surface area of the film becomes larger. When the scan rate was increased, the 3D-RGO film retained the rectangular CV shape (see Figure S6). The interconnected porous structure offers an easier way of ion diffusion, which results in a better rate capacitance. For the 3D-RGO/PANI composite film, the CV curve showed two pairs of peaks, which are attributed to the redox reaction of PANI arrays. Specifically, the peaks are ascribed to the transformation between leucoemeraldine base states and emeraldine salt (ES) states of PANI, and the transformation between ES and pernigraniline base states.[13b]

Specific capacitance can be calculated according to the equation: $C = 2(I \times t)/(m \times V)$, where C is specific capacitance ($F\ g^{-1}$), I and t are charge–discharge current and time, respectively, V is the charge voltage range, which is 0.7 V in our measurement, and m is the mass of one piece of the whole film electrode.[27] According to the equation, specific capacitances were calculated based on the galvanostatic charge–discharge curves as shown

ADVANCED MATERIALS
www.advmat.de

www.MaterialsViews.com

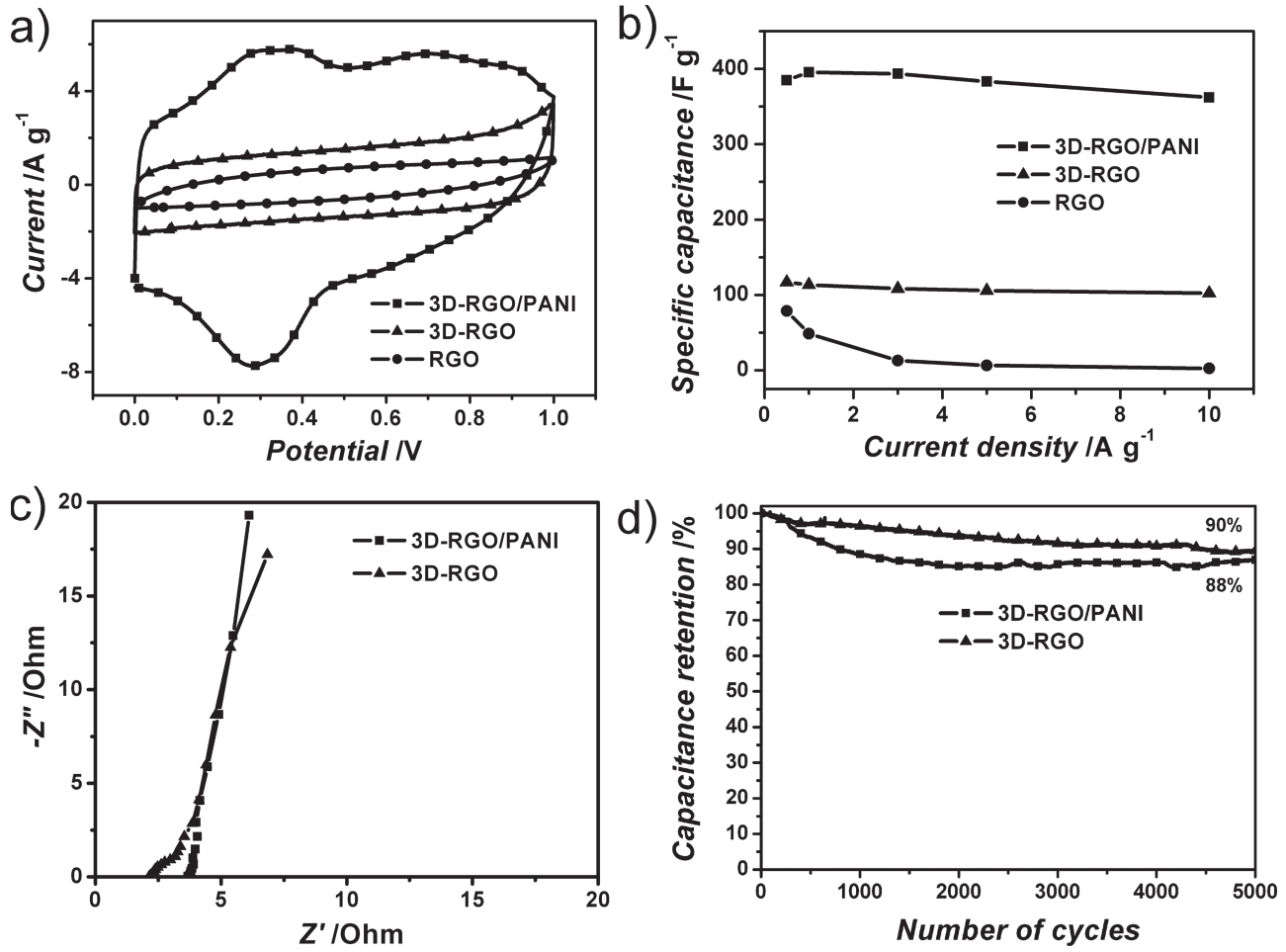

Figure 4. Electrochemical performance of the RGO film, 3D-RGO film, and 3D-RGO/PANI film. a) CV curves at scan rate of 20 mV s^{-1} in the potential range from 0 to 1 V; b) Specific capacitance at different current densities; c) Nyquist plots; d) capacitance retention over 5000 cycles at 5 A g^{-1}.

in Figure 4b for 3D-RGO (more curves for RGO and 3D-RGO/PANI are shown in Figure S7). The 3D-RGO and 3D-RGO/PANI films both maintained stable capacitance values. After the current density was changed from 0.5 to 10 A g^{-1}, 89% of the specific capacitance of the 3D-RGO film was retained. For the 3D-RGO/PANI composite film, the specific capacitance at 0.5 A g^{-1} was 385 F g^{-1}. After the current density was increased to 1 A g^{-1}, the specific capacitance of the 3D-RGO/PANI fim was 362 F g^{-1}, which indicates a capacity retention ratio of 94%. Both the capacitance and the rate performance of the film electrode are higher than those of many graphene or graphene/PANI composite films.[28] By contrast, the specific capacitance of the stack-layered RGO film decreased rapidly with increasing current density. The porous channel increased the effective surface area of graphene and afforded efficient pathways for ion diffusion, thereby enhancing the rate performance of the electrode. The formation of PANI nanowire arrays is a key factor in maintaining a high rate performance. Almost every PANI nanowire can access the electrolyte and participate in the reactions with the electrolyte due to the narrow diameters of the nanowires, and the aligned nanowires supply an optimal pathway for ion diffusion.

Nyquist plots in Figure 4c show the electrical resistance of the 3D-RGO and 3D-RGO/PANI films. Nyquist plots were obtained in the frequency range of 100 kHz to 0.05 Hz. The equivalent series resistances (Rs) of both electrodes, which can be suggested by the *x* intercept of the Nyquist plot,[10b] were 1.8 and 3.5 Ω, respectively. After formation of the composite with PANI, the Rs value increased slightly. In the high frequency areas of both plots, the negligible high-frequency resistor–capacitor loop or semicircle showed good electrode contact, which indicated a good connection between the electrode and electrolyte because of their hierarchical structures.[29] In the low-frequency part of the plot, the curves tend toward a vertical line. This result implies that the supercapacitors show almost ideal capacitive behavior, representing good ion diffusion in the electrode structure.

To further evaluate the cycle life of the composite film, galvanostatic charge–discharge measurements were carried out at a current density of 5 A g^{-1} for 5000 cycles. According to Figure 4d, 3D-RGO film kept 90% of its initial capacitance after 5000 cycles. As for the composite film of 3D-RGO/PANI, capacitance loss occurred mainly during the first 1500 cycles, and then the capacitance remained almost unchanged. The loss of

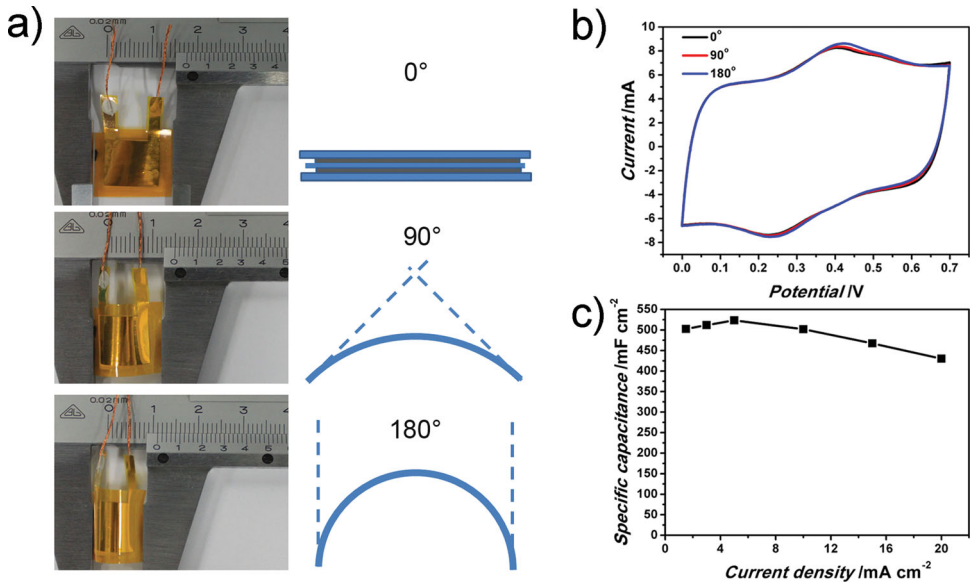

Figure 5. a) Images and schematics of a flexible film supercapacitor in different bending states; b) CV curves of the film supercapacitor at scan rates of 20 mV s^{-1} when bent by 0°, 90°, 180°. c) Area-specific capacitance of the flexible film supercapacitor under different current densities.

capacitance in the initial stage might be mainly caused by the detachment of some PANI from the RGO substrate during the charge–discharge process. After 5000 cycles, capacitance retention was 88% for 3D-RGO/PANI. The results prove good cyclic stability for both 3D-RGO and 3D-RGO/PANI film.[28a] The use of PANI nanowire arrays in RGO porous structures can release the mechanical stress at PANI–RGO interfaces during the charge–discharge process, and therefore is beneficial in maintaining the stability of the capacitance.

To test the flexibility of the film and the influence of this flexibility on electrical performance, the film was assembled into a flexible film supercapacitor by using Au-coated polyimide film as both current collector and encapsulating material. Cellulose membrane and 1 M H_2SO_4 were used as separator and electrolyte, respectively. The thickness of the whole film supercapacitor was ca. 0.2 mm. Pictures and schematics of the film supercapacitor in different bending states are shown in **Figure 5**. CV tests were carried out at 20 mV s^{-1} when the supercapacitor was bent at different angles. The film supercapacitor showed perfect CV curves in the different bending states. When the film capacitor was bent by 90° and 180°, no obvious changes in CV curves were observed, which suggests the performance of film supercapacitors based on 3D-RGO/PANI film is stable in different bending states. Moreover, the film supercapacitor exhibited a similar rate performance to that of the 3D-RGO/PANI electrode (Figure 5b). Therefore, the hierarchical film is suitable for flexible-device applications.

In summary, a novel strategy for fabricating porous graphene films is proposed. Using the suggested simple template method, a flexible free-standing graphene film with a 3D interconnected porous structure, named as 3D-RGO film, was prepared. In the 3D-RGO film, graphene sheets were stacked randomly. This film exhibited excellent supercapacitor rate performance with a retention of 89% as current density was varied from 0.5 to 10 A g^{-1}. When composed with PANI nanowire arrays, the specific capacitance reached up to 385 F g^{-1} at 0.5 A g^{-1}, with a rate retention of 94% as current density was varied from 0.5 to 10 A g^{-1}. This superior rate performance is attributed to the interconnected porous structure of the film, which allowed electrolyte ions to pass through quickly during the rapid charge–discharge process. Meanwhile, the flexible film was assembled into a flexible supercapacitor, which also exhibited excellent supercapacitor performance. This unique 3D film is a promising material as a new kind of flexible electrode for flexible or rolling-up devices.

Experimental Section

Materials: Aniline was distilled before use. All the other reagents were of analytical grade and used as received. GO was prepared from natural flaked graphite according to a modified Hummers method.[30] The process of GO production is described in the Supporting Information.

Preparation of Free-Standing 3D-RGO Film: An approximately 1.25 mg mL^{-1} GO dispersion was prepared by dispersing GO solid, which was obtained by ultrasonication for 100 min, followed by centrifugation at 4000 rpm. Free-standing 3D-RGO film was prepared by a typical process as follows: 0.4 mol $CaCl_2$ was added to 15 mL of 1.25 mg mL^{-1} GO dispersion, then 2.5 mL $NH_3{\cdot}H_2O$ were added to the mixture after $CaCl_2$ was dissolved completely. After stirring for 10 min, CO_2 gas was blown into the reaction system at a rate of 1 L min^{-1}. The reaction lasted for 80 min. After standing overnight, one third of the suspension underwent vacuum filtration to form a GO–$CaCO_3$ film. The GO–$CaCO_3$ film was reduced in hydrazine vapor at 40 °C for 12 h. The $CaCO_3$ particles were washed away by using diluted hydrochloric acid. After washing with deionized (DI) water and ethanol repeatedly, free-standing graphene films were obtained.

Preparation of 3D-RGO/PANI Composite Film: 3D-RGO/PANI nanocomposites were synthesized by dilute polymerization[17] in the presence of a 3D-RGO film. As in a typical procedure, 20 mL of 1 mol L^{-1} $HClO_4$ aqueous solution were poured into a reaction vessel in an ice bath. A piece of 3D-RGO film was placed into the vessel. 5 mL of ethanol were added to improve the wettability of the film. After the solution

was fully cooled, aniline monomer was added into the solution and stirred for 10 min to form a uniform mixture. The oxidant, $(NH_4)_2S_2O_8$ (APS), was resolved in 15 mL $HClO_4$ aqueous solution and precooled (the molar ratio of aniline/APS was 1.5). The oxidant solution was added to the monomer solution, and polymerization was started. The mixture was sustained for 24 h in an ice bath, repeatedly washed with DI water and ethanol, and dried in air, thereby yielding the composite film. Composite films were prepared at different concentrations of aniline. From experimental results (Figure S8), 0.01 mol L^{-1} proved to be the best concentration. Hence, the composed films used herein were all prepared at 0.01 mol L^{-1} of aniline.

Characterization: The as-prepared films were characterized by using SEM (Hitachi S-4800), XPS (ESCALAB250Xi), BET (Micromeritics Tristar II 3020), FTIR spectroscopy (Spectrum One), and rotation anode X-ray powder diffraction (Rigaku D/max-2500), using graphite monochromatized CuKα radiation. Electrochemical measurements were carried out in Swagelok-type cells with two symmetrical electrodes, with a glass fiber as separator (Whatman Cat No.1823 047), gold foils as current collector, and 1 m H_2SO_4 as electrolyte. The electrodes were directly cut from the films, without the use of additives. The electrochemical performances of the electrodes were characterized by CV, galvanostatic charge–discharge tests, and EIS measurements. The experiments were performed on an EG&G Princeton Applied Research VMP3 workstation. Cycle performance test was conducted on an Arbin STCS-5V1A.

Supporting Information

Supporting Information is available from Wiley Online Library or from the author.

Acknowledgements

This work was supported by the National Natural Science Foundation of China (Grant Nos. 21125420 and 91027031), the Ministry of Science and Technology of China (Grant Nos. 2009CB930400, 2010DFB63530, and 2011CB932300), and the Chinese Academy of Sciences.

Received: July 29, 2013
Published online: October 1, 2013

[1] a) J. R. Miller, A. F. Burke, *Electrochem. Soc. Interf.* **2008**, *17*, 53–57; b) P. Simon, Y. Gogotsi, *Nat. Mater.* **2008**, *7*, 845–854.
[2] a) L. L. Zhang, X. S. Zhao, *Chem. Soc. Rev.* **2009**, *38*, 2520–2531; b) A. Burke, *J. Power Sources* **2000**, *91*, 37–50; c) J. A. Rogers, Y. Huang, *Proc. Natl. Acad. Sci. U.S.A.* **2009**, *106*, 10875–10876.
[3] H. Nishide, K. Oyaizu, *Science* **2008**, *319*, 737–738.
[4] a) A. K. Geim, K. S. Novoselov, *Nat. Mater.* **2007**, *6*, 183–191; b) Y. Sun, Q. Wu, G. Shi, *Energy Environ. Sci.* **2011**, *4*, 1113; c) W. Lv, Z. Xia, S. Wu, Y. Tao, F.-M. Jin, B. Li, H. Du, Z.-P. Zhu, Q.-H. Yang, F. Kang, *J. Mater. Chem.* **2011**, *21*, 3359.
[5] a) S. Dubin, S. Gilje, K. Wang, V. C. Tung, K. Cha, A. S. Hall, J. Farrar, R. Varshneya, Y. Yang, R. B. Kaner, *ACS Nano* **2010**, *4*, 3845–3852; b) I. K. Moon, J. Lee, R. S. Ruoff, H. Lee, *Nat. Commun.* **2010**, 1–6.
[6] X. Yang, J. Zhu, L. Qiu, D. Li, *Adv. Mater.* **2011**, *23*, 2833–2838.
[7] a) A. Yu, I. Roes, A. Davies, Z. Chen, *Appl. Phys. Lett.* **2010**, *96*, 253105; b) S. Pang, Y. Hernandez, X. Feng, K. Mullen, *Adv. Mater.* **2011**, *23*, 2779–2795.
[8] a) X. Cao, Y. Shi, W. Shi, G. Lu, X. Huang, Q. Yan, Q. Zhang, H. Zhang, *Small* **2011**, *7*, 3163–3168; b) F. Liu, S. Song, D. Xue, H. Zhang, *Adv. Mater.* **2012**, *24*, 1089–1094; c) Y. Xu, K. Sheng, C. Li, G. Shi, *ACS Nano* **2010**, *4*, 4324–4330; d) C. Li, G. Shi, *Nanoscale* **2012**, *4*, 5549.
[9] Z. Chen, W. Ren, L. Gao, B. Liu, S. Pei, H. Cheng, *Nat. Mater.* **2011**, *10*, 424–428.
[10] a) Y. Zhu, S. Murali, W. Cai, X. Li, J. W. Suk, J. R. Potts, R. S. Ruoff, *Adv. Mater.* **2010**, *22*, 3906–3924; b) M. D. Stoller, S. Park, Y. Zhu, J. An, R. S. Ruoff, *Nano Lett.* **2008**, *8*, 3498–3502.
[11] a) C. Liu, F. Li, L. P. Ma, H. M. Cheng, *Adv. Mater.* **2010**, *22*, E28–62; b) Y. Yan, Y. Zhang, W. Hu, Z. Wei, *Chem. Eur. J.* **2010**, *16*, 8626–8630.
[12] a) G. Centi, S. Perathoner, *Eur. J. Inorg. Chem.* **2009**, *2009*, 3851–3878; b) M. Liu, Y.-E. Miao, C. Zhang, W. W. Tjiu, Z. Yang, H. Peng, T. Liu, *Nanoscale* **2013**, *5*, 7312–7320.
[13] a) D. Tobjork, R. Osterbacka, *Adv. Mater.* **2011**, *23*, 1935–1961; b) Y. G. Wang, H. Q. Li, Y. Y. Xia, *Adv. Mater.* **2006**, *18*, 2619–2623; c) Y.-E. Miao, W. Fan, D. Chen, T. Liu, *ACS Appl. Mater. Interfaces* **2013**, *5*, 4423–4428.
[14] J. Huang, K. Wang, Z. Wei, *J. Mater. Chem.* **2010**, *20*, 1117–1121.
[15] a) J. Xu, K. Wang, S. Z. Zu, B. H. Han, Z. Wei, *ACS Nano* **2010**, *4*, 5019–5026; b) W. Fan, C. Zhang, W. W. Tjiu, K. P. Pramoda, C. He, T. Liu, *ACS Appl. Mater. Interfaces* **2013**, *5*, 3382–3391.
[16] B. G. Choi, M. Yang, W. H. Hong, J. W. Choi, Y. S. Huh, *ACS Nano* **2012**, *6*, 4020–4028.
[17] N. R. Chiou, C. Lu, J. Guan, L. J. Lee, A. J. Epstein, *Nat. Nanotech.* **2007**, *2*, 354–357.
[18] X. C. Chen, W. Wei, W. Lv, F. Y. Su, Y. B. He, B. Li, F. Kang, Q. H. Yang, *Chem. Commun.* **2012**, *48*, 5904–5906.
[19] Z. Xu, C. Gao, *Nat. Commun.* **2011**, *2*, 571.
[20] S. Kim, S. H. Ku, S. Y. Lim, J. H. Kim, C. B. Park, *Adv. Mater.* **2011**, *23*, 2009–2014.
[21] H. Colfen, S. Mann, *Angew. Chem. Int. Ed.* **2003**, *42*, 2350–2365.
[22] H. Jiang, P. S. Lee, C. Li, *Energy Environ. Sci.* **2013**, *6*, 41.
[23] Z. Zhang, Z. Wei, M. Wan, *Macromolecules* **2002**, *35*, 5937–5942.
[24] C. Chen, Q.-H. Yang, Y. Yang, W. Lv, Y. Wen, P.-X. Hou, M. Wang, H.-M. Cheng, *Adv. Mater.* **2009**, *21*, 3007–3011.
[25] O. C. Compton, B. Jain, D. A. Dikin, A. Abouimrane, K. Amine, S. T. Nguyen, *ACS Nano* **2011**, *5*, 4380–4391.
[26] Y. Yang, M. Wan, *J. Mater. Chem.* **2002**, *12*, 897–901.
[27] M. D. Stoller, R. S. Ruoff, *Energy Environ. Sci.* **2010**, *3*, 1294.
[28] a) Q. Wu, Y. Xu, Z. Yao, A. Liu, G. Shi, *ACS Nano* **2010**, *4*, 1963–1970; b) D. W. Wang, F. Li, J. Zhao, W. Ren, Z. G. Chen, J. Tan, Z. S. Wu, I. Gentle, G. Q. Lu, H. M. Cheng, *ACS Nano*, **2009**, *3*, 1745–1752; c) Y. Xu, Z. Lin, X. Huang, Y. Liu, Y. Huang, X. Duan, *ACS Nano* **2013**, *7*, 4042–4049.
[29] a) C. Portet, M. A. Lillo-Rodenas, A. Linares-Solano, Y. Gogotsi, *Phys. Chem. Chem. Phys.* **2009**, *11*, 4943–4945; b) L. L. Zhang, X. Zhao, M. D. Stoller, Y. Zhu, H. Ji, S. Murali, Y. Wu, S. Perales, B. Clevenger, R. S. Ruoff, *Nano Lett.* **2012**, *12*, 1806–1812.
[30] W. S. Hummers, R. E. Offeman, *J. Am. Chem. Soc.* **1958**, *80*, 1339–1339.